Multi-Domain Plasma Expansion Simulations Using a Particle-in-Cell Method

Lubos Brieda[*]

Air Force Research Laboratory, Edwards AFB, CA 93524

and

Douglas VanGilder[†]

Combustion Research and Flow Technology, Pipersville, PA 18947

The statistical nature of the Particle-In-Cell (PIC) algorithm for plasma modeling requires that a large number of computational particles is used per cell to reduce the numerical noise. This requirement presents a computational obstacle in cases involving rapidly decaying plasmas, such as in simulations of plume expansion from electric propulsion (EP) thrusters. The simulation domain typically contains plasma densities ranging from 10^{17} to 10^{10} particles/m^3. Several approaches for retaining a sufficient per-cell particle count exist, including growth of simulation cells, particle splitting, and particle tracking limited to the backflowing particles, but none of these is without associated problems. In this paper, we present an alternative approach based on a multi-domain modeling. A coarse simulation is used to sample particle flux into a subdomain enclosing the region of interest. A second simulation is then performed on the subdomain, with particles injected at domain boundaries according to the prescribed flux. This approach is used to predict ion current to a simple cylindrical probe located on a satellite using a cluster of four Hall thrusters for primary propulsion. The effect of sheath resolution is investigated and results are compared to an analytical model.

I.   Introduction

The Air Force Research Laboratory (AFRL) at Edwards AFB is developing a computational package called COLISEUM[1] for modeling the interaction of electric propulsion (EP) plumes with spacecraft components. COLISEUM consists of three primary modules: RAY, AQUILA and DRACO. The RAY module is used to quickly compute line-of-sight contamination predictions, while AQUILA[2] and DRACO[3] are particle codes that track plume expansion from the source using the Particle-In-Cell (PIC)[4] method combined with MCC/DSMC[5,6] treatment of collisions.

A.   Density Decay in Particle Codes

The kinetic nature of the PIC and MCC/DSMC methods requires that a large number of particles is used per computational cell to reduce the statistical noise and to resolve the local velocity distribution function (VDF). Due to computational limitations, plasma is described by macroparticles, with each macroparticle representing w real ions. As shown in this paper and summarized in table 1, the plasma density around a typical EP spacecraft in GEO ranges from 10^{17} particles/m^3 near the thruster exit to around 10^{10} particles/m^3 in shadowed areas. Retaining a sufficient particle count per cell, N, over a density decay of seven orders of

---

[*]Research Scientist, ERC Inc., lubos.brieda.ctr@edwards.af.mil, Member AIAA
[†]Research Scientist, dvangilder@craft-tech.com, Member AIAA

American Institute of Aeronautics and Astronautics

magnitude is problematic. If the simulation cell size remains constant, N scales with density as

$$N_2 = \frac{n_2}{n_1} N_1 \tag{1}$$

region	$n(\#/\mathrm{m}^{-3})$
HET exit	10^{17}
CEX wing	$10^{12} - 10^{14}$
Wake	10^{10}

Table 1. Plasma densities encountered around a typical spacecraft flying in GEO and using a Hall Thruster for propulsion.

Retaining $N_{min} = 2$ (minimum for a DSMC collision) in the wake region, requires the simulation to track over 10 million particles per cell in the high density region near the thruster exit. Even if the wake region is deemed insignificant, and the simulation is limited to a study of CEX plasma interacting with solar arrays, the simulation needs to track around 100,000 particles per cell in the high density region. The requirement of two particles per cell is not sufficient to properly resolve the VDF, and could lead to erroneous predictions of surface sputtering.

B. Approach 1: Cell Growth

A commonly used approach in treating the density decay is allowing the cell size to grow inversely with the decay in density. This approach is used by AQUILA. While it achieves a more uniform per-cell macroparticle counts, the cell growth limits the resolution of the solution in the low density region. This is especially problematic if a detailed map of surface erosion is desired. Furthermore, unstructured codes typically use a first-order potential solver (Boltzmann-inversion or linear Poisson solver), and differentiation of the basis function results in a constant electric field per cell. This discontinuous nature of the field solution then results in an increased ion diffusion to walls due to a non-physical sheath widening.

C. Approach 2: Particle Splitting

An alternative to the use of an unstructured mesh is particle splitting. In this approach, macroparticles entering a low density region are split into two sub-particles with a halved specific weight. Although this approach increases the number of particles per cell, it does not necessarily improve the representation of the local VDF. The collision cross-section for the CEX collision in Xenon is given by Pullins[7] as

$$\sigma_{cex}\left(Xe, Xe^+\right) = 1.1872 \times 10^{-20}\left[23.3\log(g) + 188.81\right] \tag{2}$$

and collision mean free path scales as

$$\lambda_m = 1/n_n\sigma \tag{3}$$

The magnitude of relative velocity in the charge exchange wing can be approximated from neutral temperature near the thruster exit. Assuming the neutrals leave the thruster at 1000K ($\sim$ 0.1eV), the collision cross-section is 1.5×10^{-18}, leading to $\lambda_m \sim 10^6$m. Hence, the split particles will travel through the low density region on top of each other, which is analogous to the motion of the original macroparticle. Small variation in velocity can be achieved by offsetting the new born particles from the original center-of-mass trajectory. However, the effect of such random particle jumps on the simulation results in not quantified. Alternatively, the velocity of the new born particles could be adjusted such that

$$m\left(v_1' + v_2'\right) = mv \tag{4}$$

The difficulty here lies in choosing the new velocities. If the collective velocity of the incoming macroparticles can be represented by a double-Maxwellian function, then the two velocity components could be chosen from the drift and thermal components of $f_{M,1}$ and $f_{M,2}$. This approach requires each particle to track a representative VDF, which will vary as a function of position. Such a detailed treatment of particle motion is beyond the scope of standard PIC codes.

D. Approach 3: Fluid Beam Model

Additional alternative approaches were explored, of these probably the most notable is the division of the plume into the primary ion beam and the CEX wing region, as done by Roy[8] and Wang[9]. The main beam is described by an analytical profile. The kinetic treatment is limited to the charge exchange ions, and a lower macroparticle weight can be used. This approach improves the velocity representation in the low density region, however, it is not mass-conserving. This simplification could lead to an artificially high ion currents in vacuum chamber simulations, in which loss of fast ions to CEX collisions is not negligible due to the increased background neutral pressure. Furthermore, the main beam is described by an analytical profile, which is at best an approximation based on a witnessed beam divergence.

II. Multi-Domain PIC Model (MD-PIC)

A. Formulation

This paper presents a new approach for resolving the ion dynamics in a low-density region based on a multi-domain formulation. The simulation is performed in three steps, with the first two steps used to collect flux of ions into a region of interest. Then, a detailed simulation is performed on the subdomain. This approach is applicable in cases where fine details of plasma dynamics in the subdomain region do not have a strong coupling to the bulk plasma expansion. The three steps used in the process are described below.

- **Plume Expansion:** The simulation first computes the plume expansion from the thruster using a coarse mesh and a simplified geometry description. This step is identical to a typical plume/spacecraft interaction modeling. The quasi-neutral(QN) assumption generally holds, and the potential can be computed from the Boltzmann inversion,

$$\phi = \phi_0 + kT_e \ln{(n_i/n_0)} \tag{5}$$

  Collisions are treated using the MCC or DSMC approach. The simulation continues until a steady state is achieved, $dM/dt \sim 0$ and $d\bar{p}/dt \sim 0$, where M is the number of macroparticles and

$$\bar{p} = \frac{1}{M} \sum_{i=1}^{M} m_i v_i \tag{6}$$

  is the average particle momentum.

- **Flux Sampling:** Next, particle flux into the region of interest is sampled over a large number of time steps. The region of interest is typically located in a low density area, and the long sampling time is necessary to accurately capture the VDF of the incoming particles. A discrete approach is used in this method. Instead of attempting to qualify the incoming flux using an analytical profile (summation of Maxwellian functions, etc. . .), the code simply outputs the final location and velocity of each incoming particle into a file. Mass flow rate of the sampled particles is computed from

$$\dot{m} = \frac{mM_s w}{\Delta t} \tag{7}$$

  where M_s is the number of sampled particles.

- **Detailed Modeling** The last step involves detailed modeling of the low-density region. The simulation domain is limited to the subdomain enclosing the region of interest. Particles are injected into the domain using a volume source which returns a random particle from the list sampled in the previous step. Number of particles to sample each time step is computed from $\dot{m}$ calculated in the previous step. Limiting the simulation to the small subdomain provides a two-fold benefit. First, since the simulation describes a smaller physical volume, a finer cell size can be used while retaining a computationally feasible number of mesh nodes. The reduction in cell size results in an increased spatial resolution, and hence a more detailed surface mesh can be used. Second, the simulation tracks only the particles in the subdomain. The macroparticle specific weight can thus be reduced by several orders of magnitudes, resulting in a high per-cell macroparticle count.

B. Simulation Setup

The MD-PIC approach is demonstrated in this paper by modeling ion current collection by a Langmuir probe located on a hypothetical GEO spacecraft. The approach is used to investigate the importance of resolving the plasma sheath on current predictions. The spacecraft and the simulation domain are shown in figure 1(a). The spacecraft uses a cluster of four 200W Hall Effect Thrusters[10] for propulsion. Each thruster is operating at 0.8A discharge current and 250V potential. A 1.5m long beam extends from one side of the spacecraft. At the end of the beam is located a 10cm-long cylindrical probe. Due to limits of mesh resolution, the diameter of the probe was set to 5cm in the coarse simulation, which matches the diameter of the holding beam. The probe diameter was decreased to 1.2cm in the subdomain model. The extent of the subdomain is outlined by the purple boundary. Close up of the beam tip and the attached probe on the fine mesh is shown in figure 1(b). This plot also illustrates the ratio in mesh size between the coarse and the fine mesh.

(a) Simulation Domain   (b) Sub-Domain Mesh Detail
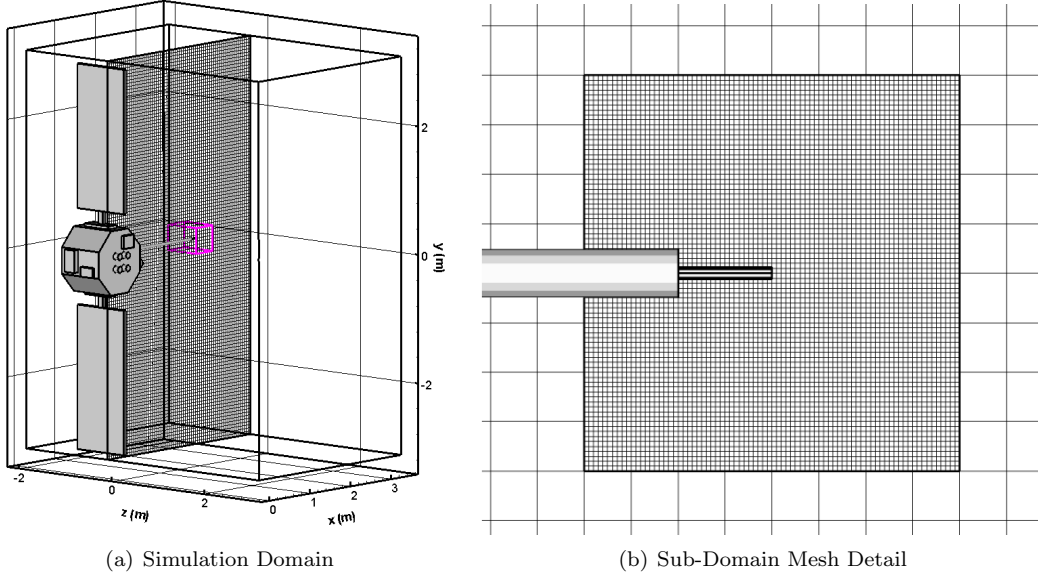
Figure 1. Simulation Setup. The hypothetical satellite contains an array of four HET thrusters, and a long beam holding a 10cm-long Langmuir probe. The region enclosed by the sub-domain is shown in purple. Figure (b) shows a close up of the probe on the fine mesh.

1. Plume Expansion

Step 1 (plume expansion) was modeled using a uniform $70 \times 123 \times 100$ mesh with $\Delta x = 0.05$m. Symmetry was assumed along the $z - y$ plane, and only half-domain was simulated. A reflective particle boundary condition was enforced on the plane of symmetry. The remaining faces were open and particles leaving through these faces were removed from the simulation. Potential was computed using the quasi-neutral approximation (eq. 5), with a constant $kT_e = 1.5$eV. Conditions at thruster exit were used to set $\phi_0 = 20$V and $n_0 = 8 \times 10^{16}$m^{-3}. The spacecraft potential was set to 0V, but the thruster was assumed to float at +20V. The simulation ran for 10,000 time steps with $\Delta t = 5 \times 10^{-7}$s. Total of 3.8 million particles were tracked at the end of the simulation.

Ions were injected using a particle source based on LIF[11] velocity distribution. The specific weight of ions was 5×10^8. Neutral mass flow rate was approximated as $\dot{m}_n = 0.1\dot{m}_i$. The simulation did not track the neutral particles, instead a steady-state distribution was modeled by loading a background neutral density by projecting the source,

$$n_n = \frac{\Gamma}{\bar{v}} \tag{8}$$

where

$$\Gamma = \int \vec{v} f_M \mathrm{d}^3 v \tag{9}$$

The CEX collisions were treated using the MCC approach. For every particle, collision frequency was calculated as

$$\nu = n_n \sigma_{CEX} g \tag{10}$$

with $g = v_i$, implying that neutral velocity is insignificant compared to the ion velocity. Collision probability,

$$P = 1 - \exp(-\nu \Delta t) \tag{11}$$

was then compared to a random number, R, and the collision was performed for $R \leq P$. The charge transfer was modeled by replacing the ion velocity with a random neutral thermal velocity,

$$v_{th} = \sqrt{\frac{2kT_n}{m_i}} f_M \tag{12}$$

where $T_n = 500K$ is a constant background neutral temperature.

2. Sampling

The particle flux into the subdomain was collected for additional 50,000 time steps. The dimensions of the subdomain were 0.4m×0.4m×0.6m and the subdomain was centered in the $x - z$ plane on the probe. The sampling resulted in collection of 74893 macroparticles, at $\dot{m} = 3.267 \times 10^{-10}$kg/s.

3. Detailed Simulation

The collected particle flux was then used to inject particles into the subdomain. This simulation used a fine mesh with $\Delta x = 0.005$m and $80 \times 80 \times 120$ cells. A detailed representation of the probe with $d = 1.2$cm was used in this case. The specific weight was decreased by $O(4)$ to 5×10^4 and the subdomain contained around 2 million particles at steady state. The effect of sheath resolution on simulated collected current was studied by computing the potential using two methods: inversion of the Boltzmann equation (QN approximation) and by solving the Poisson's equation. An $I - V$ curve was generated for both potential solvers by biasing the probe to six potential values, ϕ_b: $\phi_p - 30$V, $\phi_p - 20$V, $\phi_p - 10$V, ϕ_p, $\phi_p + 10$V and $\phi_p + 20$V, where $\phi_p = 3$V is the simulation plasma potential in the vicinity of the probe. Each simulation was executed for 5000 time steps with $\Delta t = 1 \times 10^{-7}$m/s.

III. Results

A. Results on the Coarse Mesh

Figure 2 shows the potential profile around the spacecraft obtained after 5000 time steps on the coarse mesh. The potential ranges from 20V at the thruster exit to -24V in plasma-free region. The potential near the probe tip is 3V. Despite the simulation tracking nearly 4 million particles, the potential profile is very noisy, especially in the wake on the front side of the spacecraft, and around the probe. The noise is directly related to the density decay and corresponding low macroparticle count, which are plotted in figures 3(a) and 3(b). As predicted in the introduction, number of macroparticles per cell decreased from 20,000 near the thruster to below 1 at the far extent of the CEX wing and around the probe tip.

As can be seen from figure 4(a), these results correspond to the steady-state solution, however, the low macroparticle count makes it very difficult to use the simulation results to accurately predict the ion current collection by the probe. The ion current was computed by dividing the collected current by the probe area,

$$J = \frac{I}{2\pi r l + \pi r^2} \tag{13}$$

where r is the probe radius and l is 0.1m. An attempt was made to smooth the collected data, however, as can be seen from the purple markers, smoothing did not produce any improvement in the data.
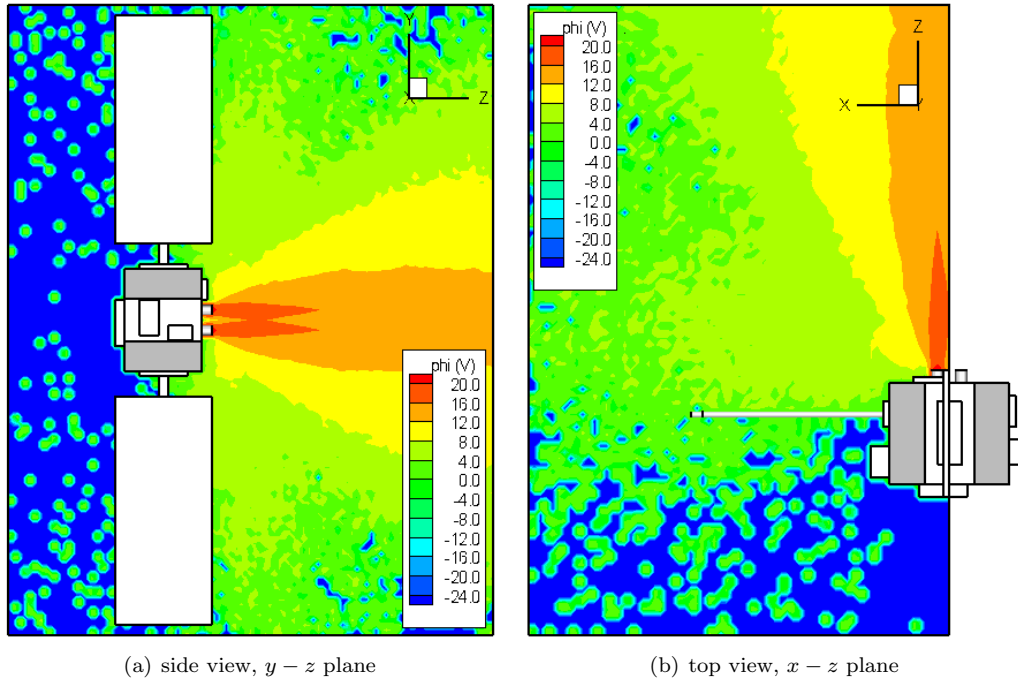
(a) side view, $y-z$ plane

(b) top view, $x-z$ plane

Figure 2. Potential profile on the coarse mesh. The simulation noise due to insufficient number of particles per cell is clearly visible.
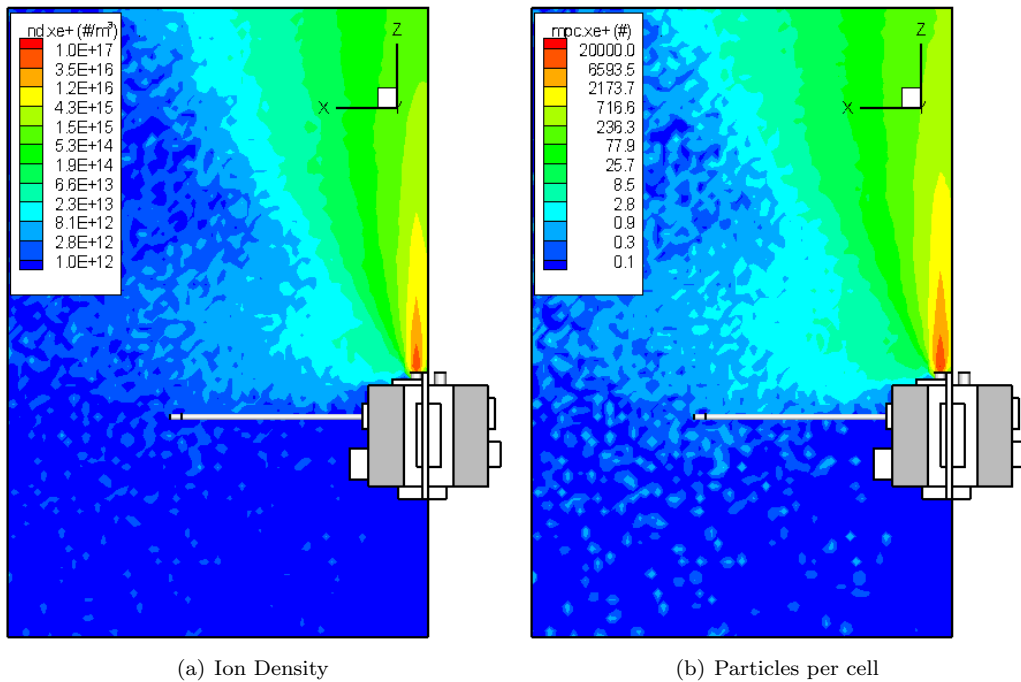

(a) Ion Density

(b) Particles per cell

Figure 3. Top view of the $x-z$ plane showing the ion density and per-cell particle count. Rapid decay in density results in the simulation tracking less than 1 particle per cell near the end of the beam holding the Langmuir probe.
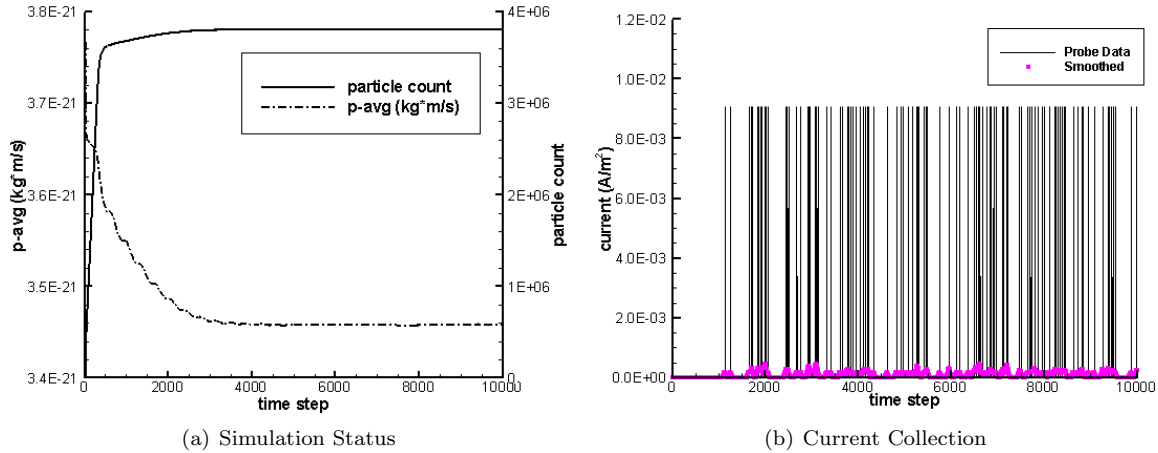
(a) Simulation Status   (b) Current Collection

Figure 4. Figure (a) shows the progression of particle count and average momentum versus time step. Both properties reach a constant value around $it = 3000$**, indicating a steady-state. Figure (b) shows the current collection by the probe versus time step. The results are very noisy due to the low particle count, and smoothing, shown by the purple markers, does not improve the results.**

B. MD-PIC Results

The continuity of solution was inspected visually, as shown in figure 5. The left plots show the potential and ion density obtained on the coarse mesh. The outline of the region covered by the subdomain is also outlined. The right plots show the corresponding solution on the subdomain. The plots show instantaneous values, obtained at corresponding steady-states, which lead to some variation in values around the border. However, both solutions display the same trends, indicating that continuity is preserved.

The coarse results indicate a significant amount of numerical noise. The noise is due to both the large simulation cell size, and the low per-cell macroparticle count. A drastic improvement can be noticed in the MD-PIC results. These results show a clear wake behind the probe, feature which is not distinguishable in the coarse simulation. The density wake results in a potential gradient around the probe. Although a similar drop can be noticed in the coarse result, it is not clear whether the drop is a steady-state prediction, or just a transient feature existing due to numerical noise. The gradient also extends over a larger physical area, which is a direct consequence of the excessively large simulation cells.

C. Effect of Sheath Resolution

The quasi-neutral approximation directly inverts the density at each node without any consideration to potential on surrounding nodes. As such, it screens out any imposed potential, and hence artificially limits the size of a sheath to the length of the simulation cell size. The DADI method, on the other hand, solves the Poisson's equation,

$$\nabla^2 \phi = -\frac{\rho}{\varepsilon_0} \tag{14}$$

and does resolve the sheath. The disadvantage of the DADI method is the additional amount of time needed to converge the iterative solver. The effect of the sheath resolution on current collection was studied by comparing the solutions obtained using the QN approximation to the DADI solution. Comparison of plasma potentials and densities is shown in strips 6(a)-6(f) and 7(a)-7(f). The top plots show the results obtained using the QN solver, while the bottom half contains the results from the DADI runs. Both solvers result in similar potential profiles, but the DADI solutions are smoother. The smoothness is due to the elliptic nature of the Poisson's equation. Important to notice is the lack of a sheath around the probe in the QN results for $\phi_b = \phi_p - 20V$ and $\phi_b = \phi_p + 20V$.

The failure to resolve the sheath leads to noticeable differences in density profiles. The QN approach results in densities nearly invariant with the applied probe potential, and wake formation is primarily due to the physical obstruction of the flow. On the other hand, the wake structure varies greatly in the DADI results. The potential applied to the probe extends to the plasma through the sheath, and increases the

(a) Potential, Coarse Mesh

(b) Potential, Subdomain

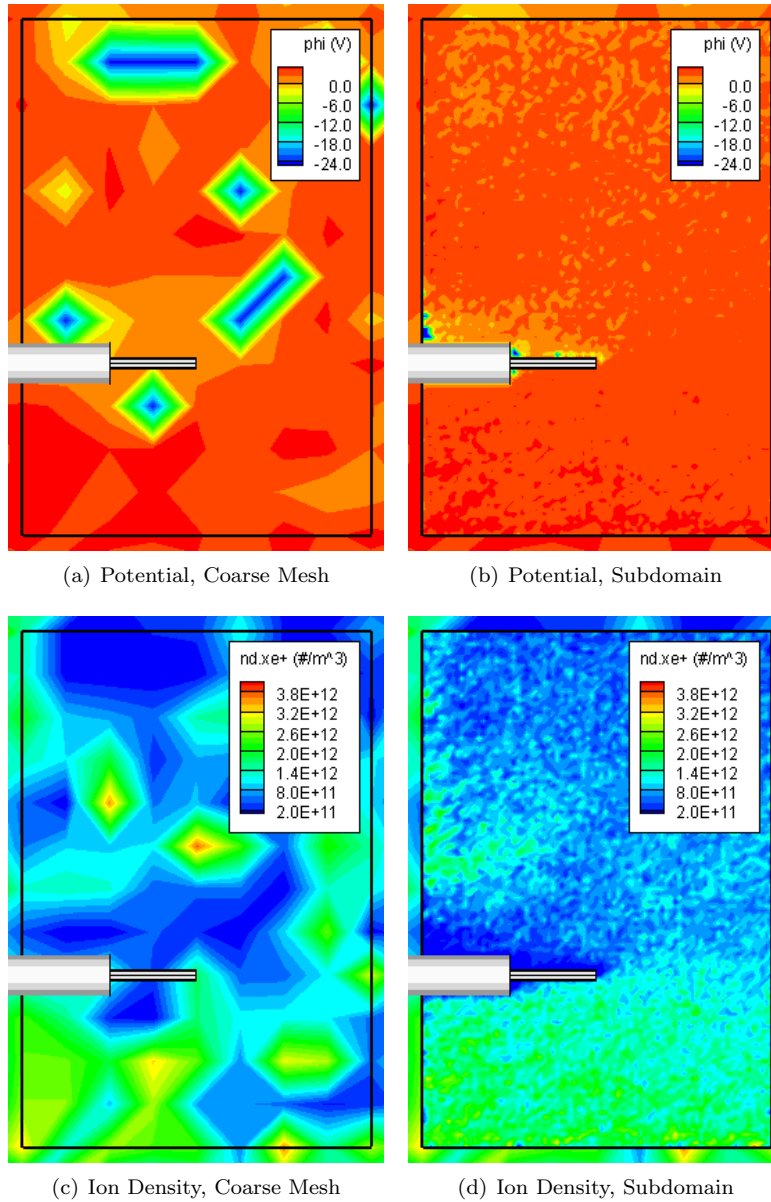(c) Ion Density, Coarse Mesh

(d) Ion Density, Subdomain

Figure 5. Continuity of solution. The plots show the instantaneous values at corresponding steady-states, which lead to some variation along the domain boundary.
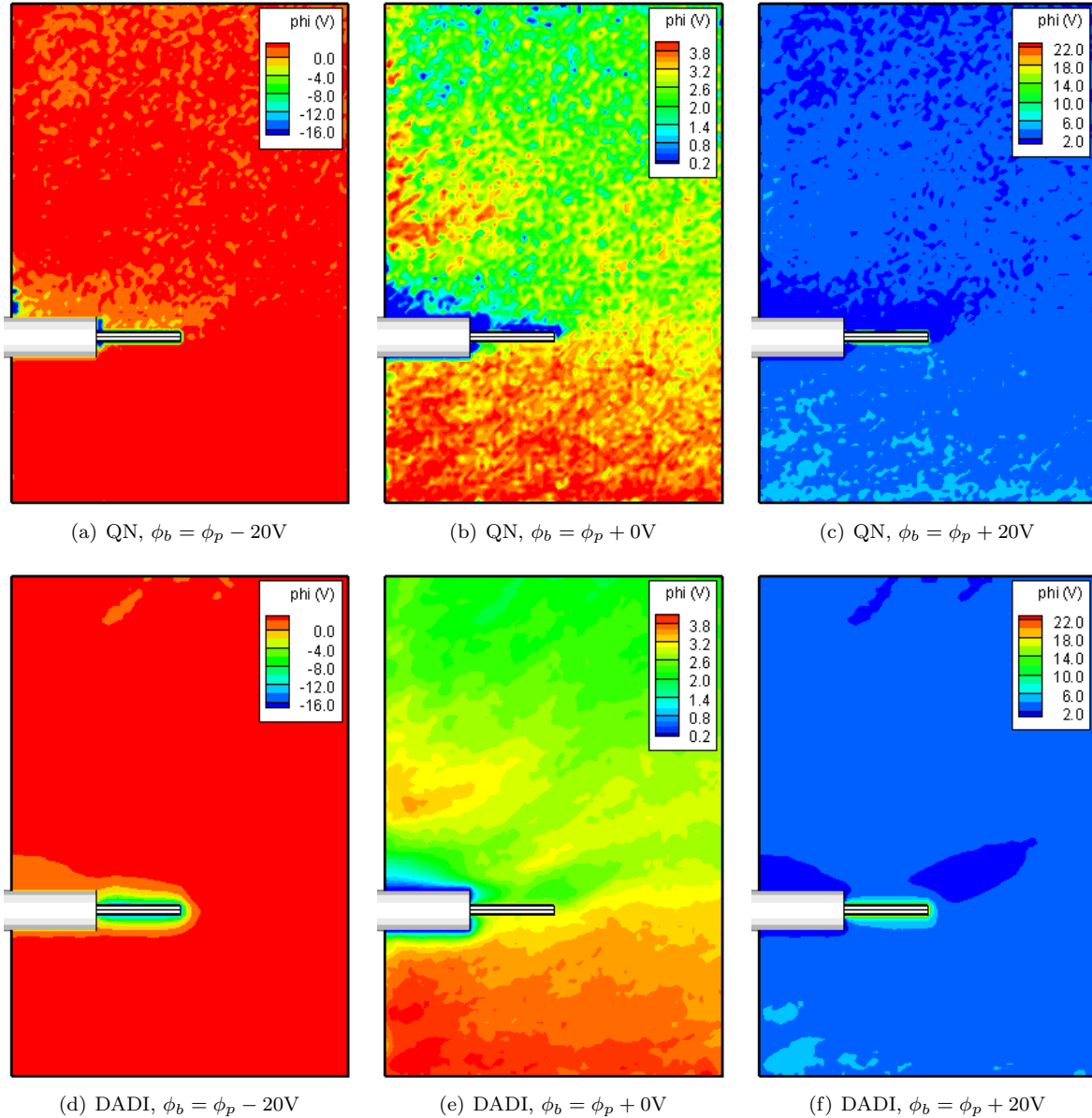
(a) QN, $\phi_b = \phi_p - 20$V

(b) QN, $\phi_b = \phi_p + 0$V

(c) QN, $\phi_b = \phi_p + 20$V

(d) DADI, $\phi_b = \phi_p - 20$V

(e) DADI, $\phi_b = \phi_p + 0$V

(f) DADI, $\phi_b = \phi_p + 20$V

Figure 6. Potential on the subdomain, obtained using the QN and DADI methods, for several probe bias potentials.

(a) QN, $\phi_b = \phi_p - 20$V

(b) QN, $\phi_b = \phi_p + 0$V

(c) QN, $\phi_b = \phi_p + 20$V

(d) DADI, $\phi_b = \phi_p - 20$V

(e) DADI, $\phi_b = \phi_p + 0$V
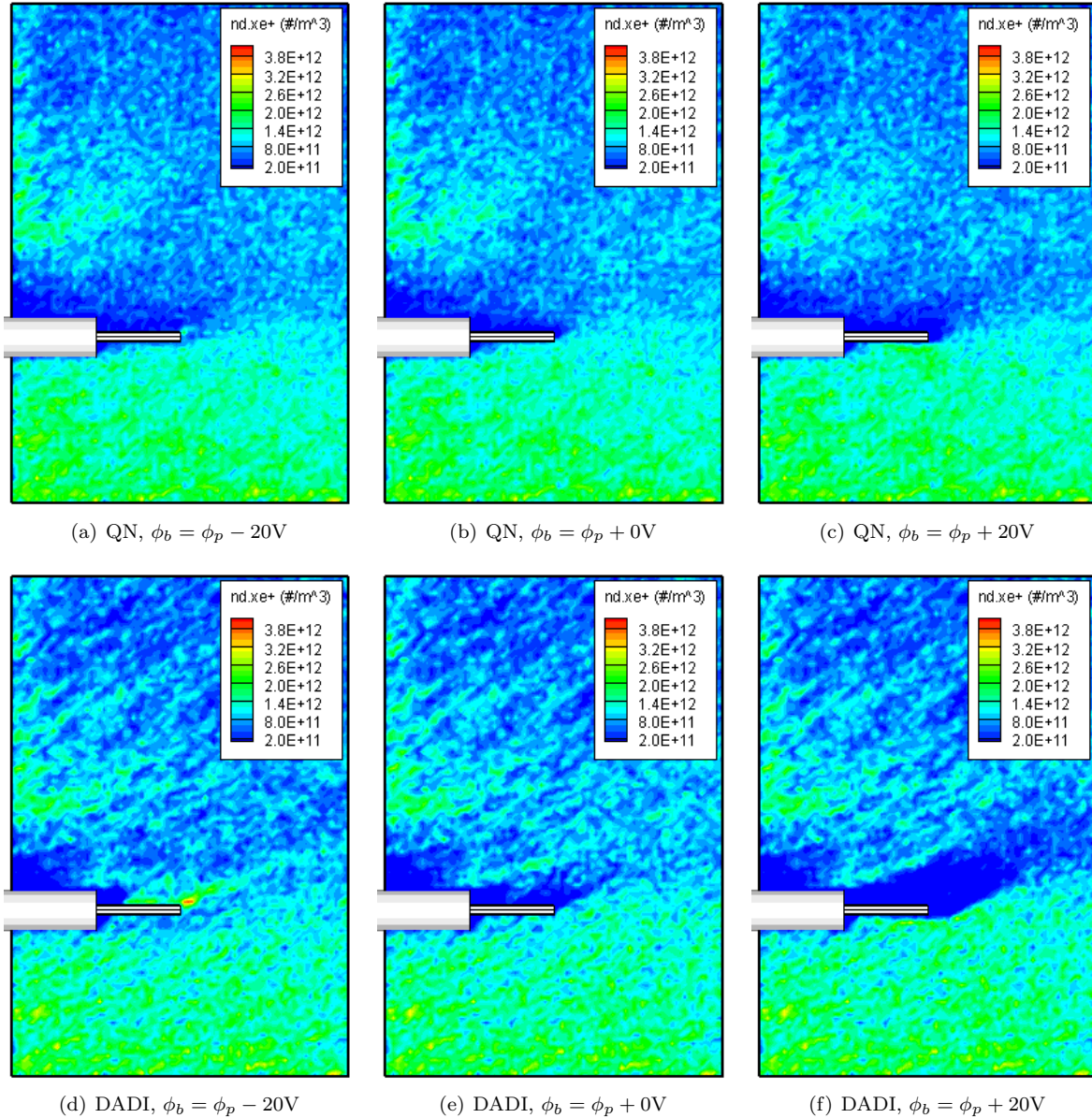
(f) DADI, $\phi_b = \phi_p + 20$V

Figure 7. Ion density on the subdomain, obtained using the QN and DADI methods, for several probe bias potentials.

effective probe area. Large negative bias leads to an increase in plasma density around the probe. The wake is almost non-existent, as the slow moving CEX ions are attracted back to the probe. Important to note is the similarity between the two solvers for the $\phi_b = \phi_p$ case. This result was expected, since at this condition the probe is biased to the plasma potential, and subsequently, there is no sheath. The positive probe bias results in repulsion of ions from the probe. The probe is biased to +20V from the surrounding plasma, and hence only particles with KE≥20V have sufficient energy to reach it. Since the CEX ions are born nearly at rest (neutral thermal velocity), and the potential drop between the thruster and the probe is ≤17V, this bias should result in no current collection.

This is indeed the case, as can be seen from the ion current plots in figure 8(a). The green line indicates the current collected versus the time step for $\phi_b = \phi_p + 20V$. No statistically significant current is sampled. As expected, an overlap is seen between the black dotted and the black solid lines. The dotted lines correspond to the DADI results, while the solid line shows the current obtained from the QN approximation. The black lines indicate the ion current at the floating potential, $\phi_b = \phi_p$. Since this condition does not result in formation of a sheath, the lack of sheath resolution by the QN method is trivial. A strong dependence on sheath resolution is seen in the plot for the negative probe bias. The potential gradient in the sheath modifies the trajectory of particles that would otherwise flow past the probe, and hence the DADI case results in a higher current collection. The results are summarized in the $I - V$ curve plotted in figure 8(b). As can be seen, the probe starts repelling ions at $\phi_b > 10V$. The QN case under-predicts the current due to screening of applied potential at length scales larger than the cell.

The two MD-PIC results were also compared to a theoretical model of Prokopenko and Laframboise,[12] given by

$$ j_{pl} = j_0 \left[2 \left(Q/\pi \right)^{1/2} + \exp \left(Q \right) \mathrm{erfc} \left(Q^{1/2} \right) \right] \tag{15} $$

where

$$ Q = -q\phi_b/kT_e \tag{16} $$

This relationship, derived assuming an infinitely long cylinder, the *thick-sheath* limit and uniform mono-energetic beam at infinity, scales with kT_e and j_0. The comparison was performed using $kT_e = 1.5eV$ and $j_0 = j_{QN}(+0V)$. An agreement within an order of magnitude is seen between the model and both simulation results, however, the DADI case results in a significant error reduction, and a comparable I vs. V behavior. The trend seen in the QN curve corresponds to kT_e of 12eV. The discrepancies in magnitude could be attributed to a limited applicability of this model to the simulated case.
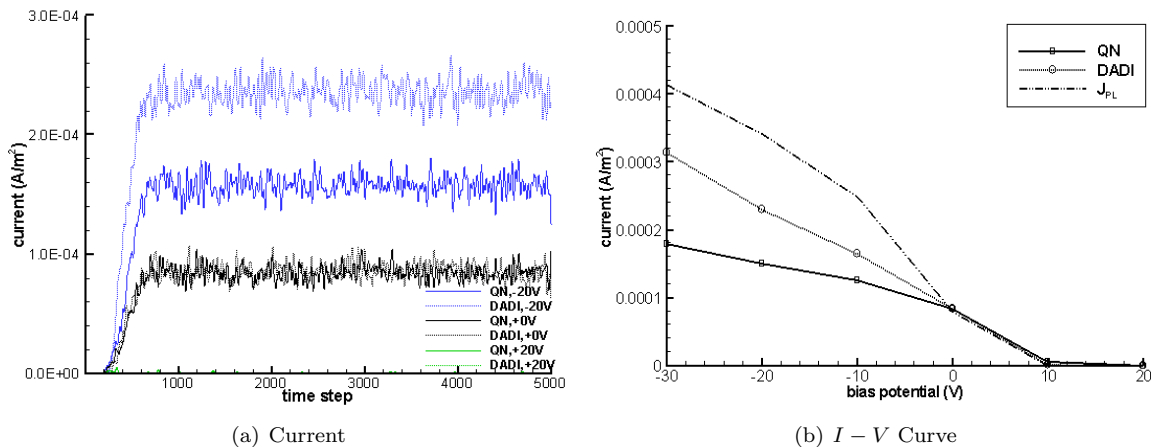

(a) Current

(b) $I - V$ Curve

Figure 8. Probe current collection determined by the MD-PIC approach. Figure (b) shows the $I - V$ curve for the ion current.

IV.   Conclusion and Future Work

A multi-domain approach (MD-PIC) for resolving ion dynamics in low-density regions was presented in this paper. This approach is based on a three step modeling approach, with the first two steps used to sample

particle flux into a region of interest. Detailed simulation on the subdomain is then performed, utilizing a reduced cell size, refined surface geometry, and a lower macroparticle specific weight. The MD-PIC approach was used in this paper to study the effect of sheath resolution on collection of ion current by a Langmuir probe located on a hypothetical EP GEO spacecraft. An $I - V$ curve was obtained using six probe bias potentials. Current collection demonstrated a strong dependence on the sheath resolution for all negative bias potentials. The quasi-neutral case, which does not resolve the sheath, under-predicted the current collection, due to the reduced collection area associated with the numerical screening of potential gradient at length scales larger than the cell. Simulation results were also compared to a theoretical model, and an agreement within 30% was achieved for the Poisson solver case.

These results indicate that sheath resolution is critical in cases where a detail prediction of surface ion collection is needed. The sheath increases the effective collection area, and hence increases the collected particle flux. The potential profile within the sheath also alters the trajectory of the incoming particles. Correct prediction of incident angle is important in sputtering analysis, as sputter yield shows a strong dependence on incident angle. The MD-PIC approach provides the capability to resolve the sheath in the region of interest, while retaining a high per-cell particle count. As such, this approach is applicable to studies of surface erosion, spacecraft charging, and detailed modeling of plasma probes. In the future, an attempt will be made to further validate the model through a comparison with published in-flight sensor measurements.

Acknowledgments

References

[1]Gibbons, M., et. al., "Flexible Three-Dimensional Modeling of Electric Thrusters in Vaccum Chambers," *AIAA/ASME/SAE/ASEE Joint Propulsion Conference and Exhibit*, 2003

[2]Santi, M., Cheng, S., Celik, M., Martinez-Sanchez, M., and Peraire, J., "Further Development and Preliminary Results of the Aquila Hall Thruster Plume Model," AIAA-2003-4873, 2003

[3]Brieda, L., Pierru, J., Kafafy, R., and Wang, J., "Development of the DRACO Code for Modeling Electric Propulsion Plume Interactions," *AIAA/ASME/SAE/ASEE Joint Propulsion Conference and Exhibit*, 40th, Fort Lauderdale, FL, July 11-14, 2004

[4]Birdsall, C., and Langdon, A., *Plasma Physics Via Computer Simulations*, Institute of Physics Pub., Philadelphia, 2000

[5]Birdsall, C.K., "Particle-in-Cell Charged-Particle Simulations, Plus Monte Carlo Collisions With Neutral Atoms, PIC-MCC," *IEEE Transactions on Plasma Science*, Vol.19, No.2, pp.65-85

[6]Bird, G. A., *Molecular Gas Dynamics and the Direct Simulation of Gas Flows*, Oxford University Press, Oxford, 2003

[7]Pullins, S., Chiu, Y.H., Levandier, D.J, and Dressler, R.A., "Ion Dynamics in Hall Effect and IOn Thrusters - $Xe^+ + Xe$ Symmetric Charge Transfer," *38th Aerospace Sciences Meeting and Exhibit*, Reno, NV, January 10-14, 2000

[8]Roy, S.R., "Numerical Simulation of Ion Thruster Plume Backflow for Spacecraft Contamination Assesment," Ph.D. Dissertation, Aeronautics and Astronautics Dept., Mass. Institute of Technology, Cambridge, MA, 1985

[9]Wang, J., Brinza, D., Young, M., "Three-Dimensional Particle Simulations of Ion Propulsion Plasma Environment for Deep Space 1," *Journal of Spacecraft and Rockets*, Vol. 38, No. 3, 2001.

[10]Hargus, W., Reed, G., "The Air Force Clustered Hall Thruster Program,", *AIAA/ASME/SAE/ASEE Joint Propulsion Conference and Exhibit*, 38th, Indianapolis, IN, July 7-10, 2002

[11]Hargus, W., Charles, Lt. C., "Near Exit Plane Velocity Field of a 200W Hall Thruster," *AIAA/ASME/SAE/ASEE Joint Propulsion Conference and Exhibit*, 39th, Huntsville, AL, July 20-23, 2003

[12]Hastings, D., and Garrett, H., *Spacecraft-Environment Interactions*, Cambridge University Press, Cambridge, England, 1996